Constitutive Behavior of AA5050/MgO Metal Matrix Composites with Interface Debonding: the Finite Element Method for Uniaxial Tension

A. Chennakesava Reddy

Assistant Professor, Department of Mechanical Engineering, MJ College of Engineering and Technology, Hyderabad, India
dr_acreddy@yahoo.com

Abstract: *A square array unit cell/hexagonal* MgO *nanoparticle RVE models were used to predict micromechanical behavior and interfacial debonding in AA5050/* MgO *composites. The AA5050/* MgO *particulate metal matrix composites were fabricated at different volume fractions of* MgO. *Partial agglomeration was observed in composites with high content of MgO. The tensile strength of composites decreased by increasing the large content of MgO. The interfacial debonding was happened in all the composites.*

Keywords: AA5050*, magnesium oxide, hexagonal nanoparticle, RVE model, finite element analysis, debonding.*

1. INTRODUCTION

Debonding of particle/matrix interfaces in composites may significantly affect their macroscopic behavior since interface debonding leads to crack initiation and propagation. Interface debonding is usually characterized by a nonlinear cohesive law(e.g., Needleman [1] ; Tvergaard and Hutchinson [2]; Camacho and Ortiz [3]; Zhong and Knauss [4]; Espinosa et al. [5]; Geubelle and Baylor [6], which gives the stress tractions in terms of displacement discontinuities across the interface. A study was conducted on the silane interfacial effect on the fracture process of embedded single E-glass fiber [7]. The interfacial reinforcement reflects the progressed fracture rather than the instantaneous fracture. Various kinds of ceramic materials, e.g. silicon nitride [8, 9], titanium oxide [10, 11], graphite [12], titanium carbide [13, 14], boron nitride [15], zirconium oxide [16], titanium nitride [17], titanium boride [18], zirconium carbide [19], silicon oxide [20], magnesium oxide [21], are extensively used to reinforce aluminum alloy matrixes. Recently the interface debonding was studied in composites subject to uniaxial tension since it is a widely used test to characterize the material behavior. [7-21].

Magnesium oxide (MgO) is a refractory material with melting point of about 2780°C. MgO possesses good properties such as the good thermal shock resistance, high melting point, low thermal conductivity, and excellent thermodynamic stability. Its density, Young's modulus, and hardness are 3.5 g/cm^3, 320 GPa, and 910 HV, respectively. In this study, nano MgO particles were used to reinforce AA5050 alloy by stir casting process. The micromechanical behavior was also simulated using finite element method. The shape of TiC particle considered in this work is a hexagonal. The periodic particle distribution was a square array as shown in figure 1.

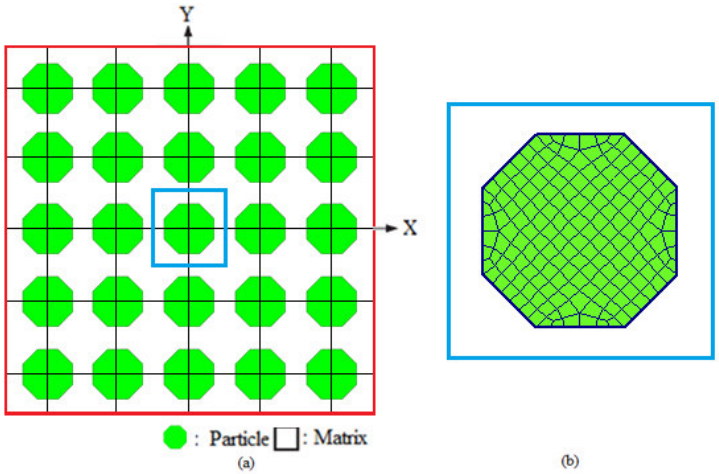

Figure 1: A diamond RVE containing an ellipsoidal nanoparticle.

2. THEORETICAL BACKGROUND

The strains along x- and y-directions can be determined as using the following equations:

$$\varepsilon_y = -\left(\frac{v_{xy}}{E_x} + \frac{1}{E_z}\right)P = \frac{\Delta y}{a} \quad (1)$$

$$\varepsilon_x = \left(\frac{1}{E_x} - \frac{1}{E_z}\right)P = \frac{\Delta x}{a} \quad (2)$$

The effective elastic moduli and Poisson's ratio in the transverse direction (xy-plane) as follows:

$$E_x = \frac{1}{\frac{\Delta x}{Pa} + \frac{1}{E_z}} \text{ and } E_y = \frac{1}{\frac{\Delta y}{Pa} + \frac{1}{E_z}} \quad (3)$$

$$v_{xy} = \left(\frac{\Delta y}{Pa} + \frac{1}{E_z}\right)/\left(\frac{\Delta x}{Pa} + \frac{1}{E_z}\right) \quad (4)$$

Once the change in lengths along x- and y- direction (Δx and Δy) are determined for the square RVE from the FEA, E_y and E_x and v_{xy} can be determined from Eqs. (3) and (4), correspondingly. Considering adhesion, formation of precipitates, particle size, agglomeration, voids/porosity, obstacles to the dislocation, and the interfacial reaction of the particle/matrix, the formula for the strength of composite is stated below:

$$\sigma_c = \left[\sigma_m \left\{\frac{1-(v_p+v_v)^{2/3}}{1-1.5(v_p+v_v)}\right\}\right] e^{m_p(v_p+v_v)} + kd_p^{-1/2} \quad (5)$$

$$k = E_m m_m / E_p m_p$$

where, v_v and v_p are the volume fractions of voids/porosity and nanoparticles in the composite respectively, m_p and m_m are the possion's ratios of the nanoparticles and matrix respectively, d_p is the mean nanoparticle size (diameter) and E_m and E_p is elastic moduli of the matrix and the particle respectively. Elastic modulus (Young's modulus) is a measure of the stiffness of a material and is a quantity used to characterize materials. Elastic modulus is the same in all orientations for isotropic materials. Anisotropy can be seen in many composites.

The upper-bound equation is given by

$$\frac{E_c}{E_m} = \left(\frac{1-v_v^{2/3}}{1-v_v^{2/3}+v_v}\right) + \frac{1+(\delta-1)v_p^{2/3}}{1+(\delta-1)(v_p^{2/3}-v_p)} \quad (6)$$

The lower-bound equation is given by

$$\frac{E_c}{E_m} = 1 + \frac{v_p - v_p}{\delta/(\delta-1)-(v_p+v_v)^{1/3}} \quad (7)$$

where, $\delta = E_p/E_m$.

The transverse modulus is given by

$$E_t = \frac{E_m E_p}{E_m + E_p(1-v_p^{2/3})/v_p^{2/3}} + E_m\left(1 - v_p^{2/3} - v_v^{2/3}\right) \quad (8)$$

3. MATERIALS METHODS

The matrix material was AA4015 alloy. The reinforcement material was ellipsoidal TiC nanoparticles of average size 100nm. The mechanical properties of materials used in the present work are given in table 1.

Table 1: Mechanical properties of AA5050 matrix and MgO nanoparticles

Property	AA5050	MgO
Density, g/cc	2.69	3.54
Elastic modulus, GPa	68.90	320.00
Ultimate tensile strength, MPa	172	
Poisson's ratio	0.33	0.35

AA5050 alloy/MgO composites were manufactured by the stir casting process and low pressure casting technique with argon gas at 3.0 bar. The composite samples were give solution treatment and cold rolled to the predefined size of tensile specimens. The heat-treated samples were machined to get flat-rectangular specimens (figure 2) for the tensile tests. The tensile specimens were placed in the grips of a Universal Test Machine (UTM) at a specified grip separation and pulled until failure. The test speed was 2 mm/min (as for ASTM D3039). A strain gauge was used to determine elongation.

In this research, a cubical representative volume element (RVE) was implemented to analyze the tensile behavior AA5050/ MgO nanoparticle composites at three (10%, 20% and 30%) volume fractions of MgO. The large strain PLANE183 element

was used in the matrix in all the models. In order to model the adhesion between the matrix and the particle, a CONTACT 172 element was used.

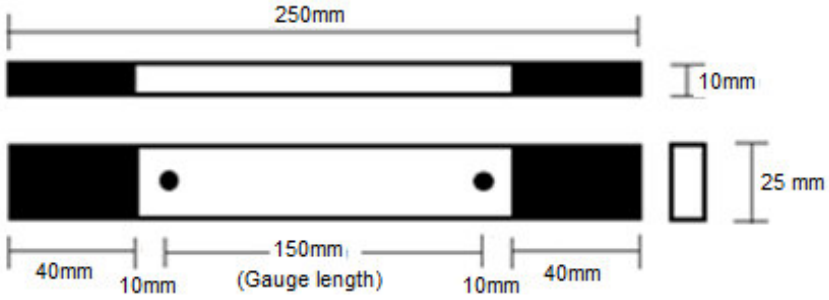

Figure 2: Shape and dimensions of tensile specimen

4. RESULTS AND DISCUSSION

Figure 3 shows the XRD of the MgO calcinated at 400°C, it is clearly observed that the highest intensity peak is obtained at (200) crystal planes of MgO with FCC phase (lattice constant a of cubic unit cell: 0.421 nm), owing to diffraction peaks assigned to (111), (200) and (220) crystal planes. The sharp diffraction peaks were clearly seen and they are perfectly matches with crystal structure of MgO, therefore, crystallinity of MgO particles is obvious having average crystalline size in nano order.

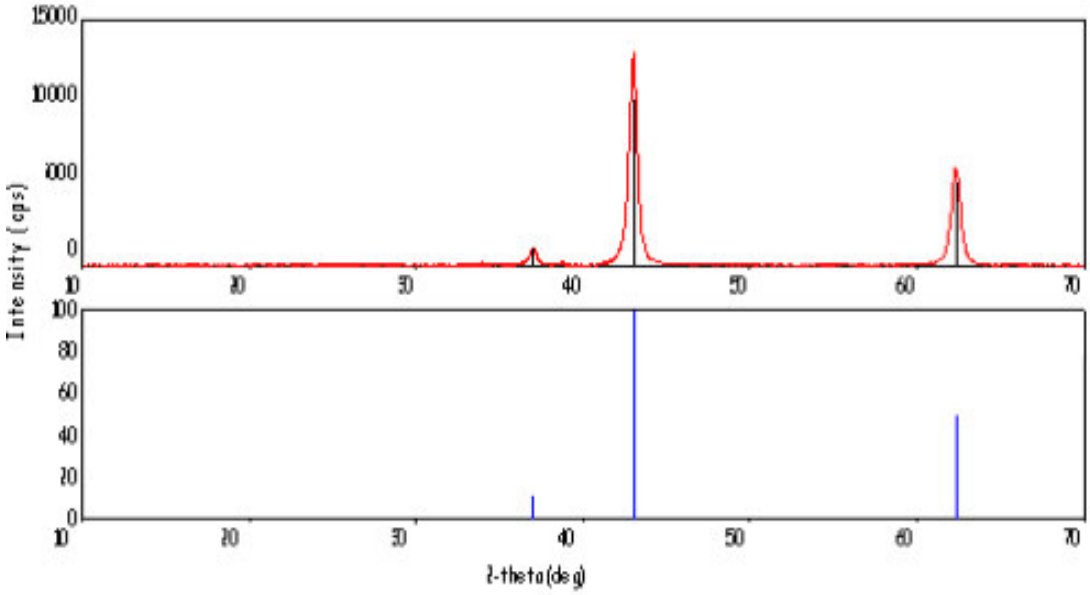

Figure 3: XRD of Magnesium Oxide.

4.1 Micromechanical Behavior

Figure 4a represents the normalized tensile strengths of the AA5050 alloy/ MgO composites obtained by FEA, present mathematical model, and experimental test. The tensile strength is normalized with ultimate tensile strength of AA5050 alloy. The results obtained from present mathematical model are established with the experimental values. The difference between the results obtained from experimental procedure and the FEA is due to the ignorance of porosity in the matrix, uniform distribution of MgO particles and agglomeration of MgO particles. Scanning electron microstructure of composites with the content of 30 vol.% MgO is shown in figure 5. Dark Al matrix and bright particles of MgO can be clearly observed. The phases are indicated by arrows on images. It should be noted that nano-sized MgO particles were well dispersed in the matrix of aluminum and just a partial agglomeration in composites with high content of MgO. With increasing the volume fraction of magnesium oxide particles in the constant particle size, the distances between particles decreases and resulted in enhancement of dislocation density and their pile-ups behind the MgO particles; therefore, higher stress needs to move dislocations, which also has the effect on strength increment. It should be noted that the porosities develop discontinuity in the samples and act as stress concentration locations and cause severe decreases in samples properties. On the other hand, with increasing amount of reinforce-

ment particles, homogeneity in distribution of magnesium oxide particles in the matrix decreased and in some areas formed the cluster assembly. Therefore, the effects of MgO particles by direct contact with each other and lack of the strong mechanical bonding between them, decreases tensile strength as seen from FEA results. Process of strength reduction in composite samples with 30 vol.% of MgO particles is more visible.

The normalized elastic modulus is shown in figure 4b. The elastic modulus is normalized with the elastic modulus of AA5050 alloy. The stiffness of the composites increases with increase of volume fraction of Mgo. The upper limit (UL) values computed by the present mathematical model are higher than those values obtained by the 'Role of Mixtures (ROM)'and FEA. This is because of assumption of voids in the present mathematical model. The shear strength of the composites decreases with increase of volume fraction of MgO (figure 4c). The major Poisson's ratio increases with increase of volume fraction of MgO particles (figure 4d).

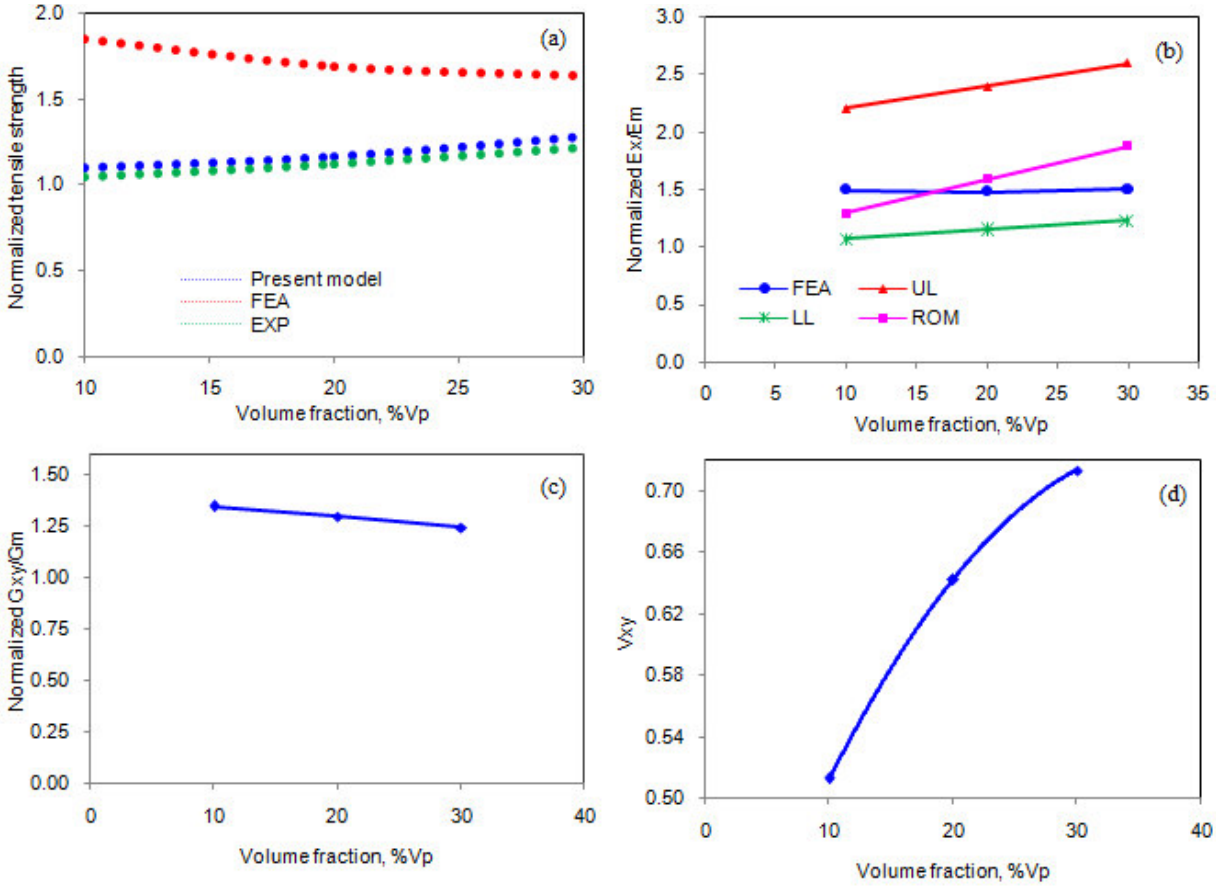

Figure 4: Effect of volume fraction on micromechanical behavior of AA5050/MgO composites.

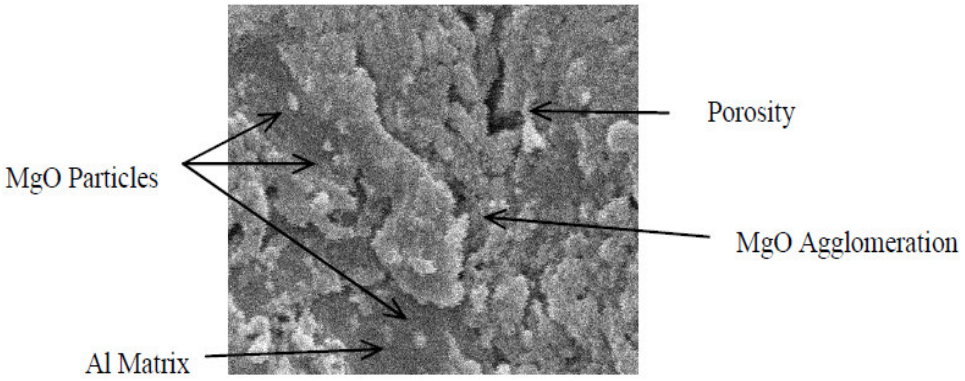

Figure 5: SEM image of composite containing 30 vol. % MgO.

4.2 Fracture Analysis

If the particle deforms in an elastic manner (according to Hooke's law) then,

$$\tau = \frac{n}{2}\sigma_p \quad (9)$$

where σ_p is the particle stress. If particle fracture occurs when the stress in the particle reaches its ultimate tensile strength, $\sigma_{p,uts}$, then setting the boundary condition at

$$\sigma_p = \sigma_{p,\,uts} \quad (10)$$

The relationship between the strength of the particle and the interfacial shear stress is such that if

$$\sigma_{P,uts} < \frac{2\tau}{n} \quad (11)$$

Then the particle will fracture. From the figure 6b, it is observed that the MgO nanoparticle was not fractured as the condition in Eq. (11) is not satisfied. For the interfacial debonding/yielding to occur, the interfacial shear stress reaches its shear strength:

$$\tau = \tau_{max} \quad (12)$$

For particle/matrix interfacial debonding can occur if the following condition is satisfied:

$$\tau_{max} < \frac{n\sigma_p}{2} \quad (13)$$

It is observed from figure 6a that the interfacial debonding occurs between MgO nanoparticle and AA5050 alloy matrix as the condition in Eq.(13) is satisfied.

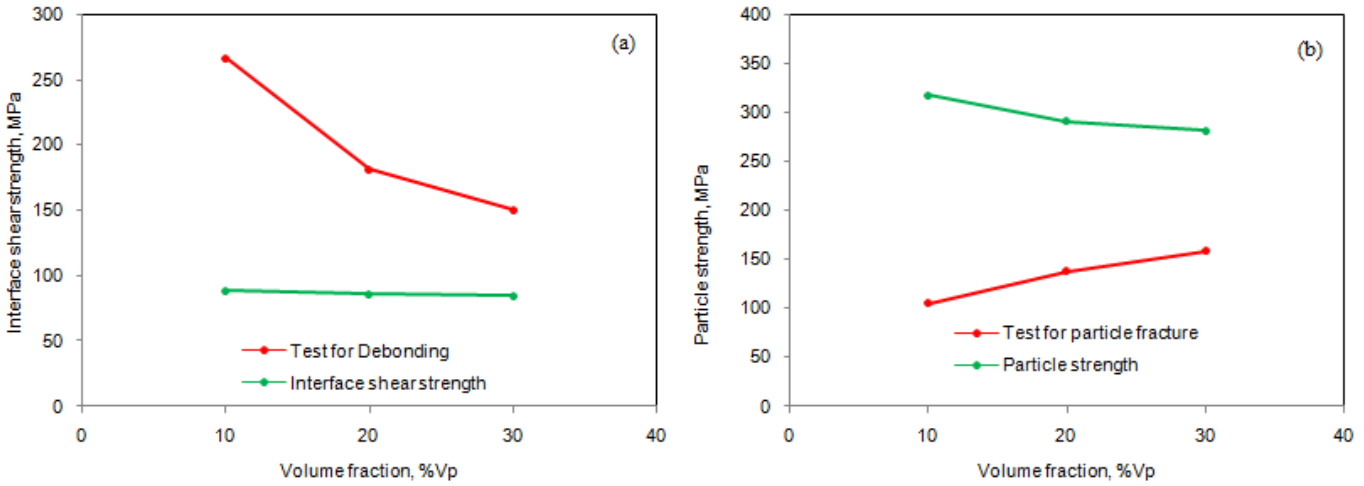

Figure 6: Criterion interfacial debonding (a) and for particle fracture (b).

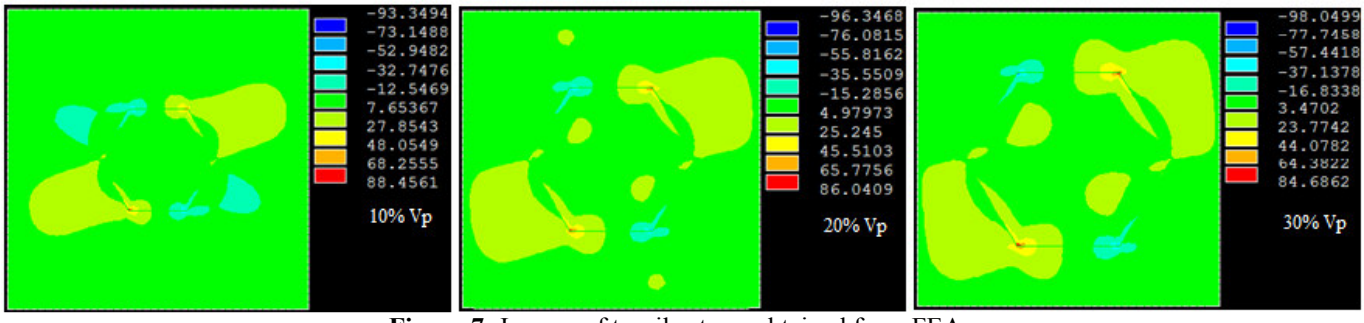

Figure 7: Images of tensile stress obtained from FEA.

As seen from figure 7, the shear stress developed at the interface are higher than that induced in the nanoparticle. Hence, the interfacial debonding was occurred between the particle and the matrix. The matrix fracture is also observed in AA5050/ MgO composites due to inadequate transfer of load from the matrix to the particle (figure 8) at high volume fraction of MgO.

The ceramic particles can only deform elastically while aluminum matrix can deform plastically. So if the boundary is assumed to be strong, ceramic particles prevent plastic deformation of the matrix and this leads to higher work-hardening rate. The difference between elastic moduli of ceramic and metal matrix may result in stress concentrations resulting high density of dislocations.

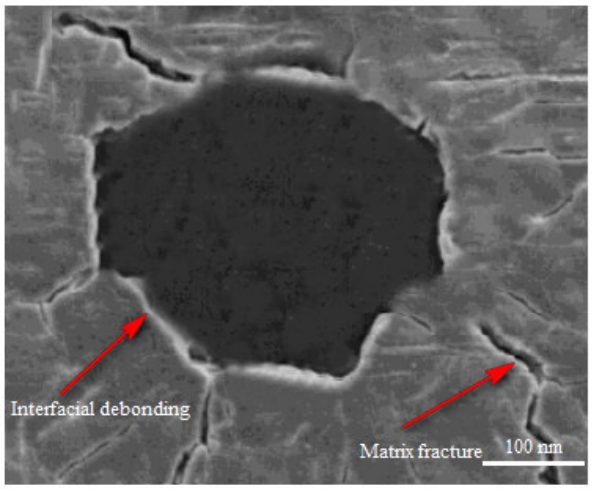

Figure 8: SEM images illustrating interfacial debonding matrix fracture in the composite containing 30% MgO.

5. CONCLUSION

SEM micrographs indicate that reinforcement particles were homogeneously distributed in the matrix of composites. However, partial agglomeration was observed in composites with high content of MgO. The tensile strength of composites decreased by increasing the large content of MgO. The interfacial debonding was happened in all the composites and the matrix fracture was occurred in the composites containing high volume fraction of MgO.

REFERENCES

1. A. Needleman, A continuum model for void nucleation by inclusion debonding, Journal of Applied Mechanics, 54, 1987, pp.525–531.
2. V. Tvergaard, J. W. Hutchinson, The relation between crack growth resistance and fracture process parameters in elastic-plastic solids, Journal of the Mechanics and Physics of Solids, 40, 1992, pp. 1377–1397.
3. G. T. Camacho, M. Ortiz, Computational modelling of impact damage in brittle materials, International Journal of Solids and Structures, 33, 1996, pp. 899–2938.
4. X. A. Zhong, W. G. Knauss, Analysis of interfacial failure in particle-filled elastomers, Journal of Engineering Materials and Technology, 119, 1997, pp. 98–204.
5. H. D. Espinosa, P. D. Zavattieri, S. K. Dwivedi, A finite deformation continuum/discrete model for the description of fragmentation and damage in brittle materials, Journal of the Mechanics and Physics of Solids 46, 1998, pp. 1909–1942.
6. P. H. Geubelle, J. S. Baylor, Impact-induced delamination of composites: a 2D simulation, Composites, B29, 1998, pp. 589–602.
7. B. Kotiveerachari, A. Chennakesava Reddy, Interfacial effect on the fracture mechanism in GFRP composites, CEMILAC Conference, Ministry of Defence, India, 20-21st August 1999.
8. A. Chennakesava Reddy, Assessment of Debonding and Particulate Fracture Occurrences in Circular Silicon Nitride Particulate/AA5050 Alloy Metal Matrix Composites , National Conference on Materials and Manufacturing Processes, Hyderabad, India, 27-28 February 1998, pp. 104-109.
9. A. Chennakesava Reddy, Evaluation of Debonding and Dislocation Occurrences in Rhombus Silicon Nitride Particulate/AA4015 Alloy Metal Matrix Composites, 1st National Conference on Modern Materials and Manufacturing , Pune, India, 19-20 December 1997, pp. 278-282.
10. S. Sundara Rajan, A. Chennakesava Reddy, Deformation Behavior of AA8090/ TiO_2 Nanoparticulate Reinforced Metal Matrix Composites with Debonding Interfaces, 2nd International Conference on Composite Materials and Characterization, Nagpur, India, 9-10 April 1999, pp. 245-248.
11. A. Chennakesava Reddy, Cohesive Zone Finite Element Analysis to Envisage Interface Debonding in AA7020/Titanium Oxide Nanoparticulate Metal Matrix Composites , 2nd International Conference on Composite Materials and Characterization, Nagpur, India, 9-10 April 1999, pp. 204-209.
12. A. Chennakesava Reddy, Micromechanical Modelling of Interfacial Debonding in AA1100/Graphite Nanoparticulate Reinforced Metal Matrix Composites, 2nd International Conference on Composite Materials and Characterization, Nagpur, India, 9-10 April 1999, pp. 249-253.

13. A. Chennakesava Reddy, Local Stress Differential for Particulate Fracture in AA2024/Titanium Carbide Nanoparticulate Metal Matrix Composites, National Conference on Materials and Manufacturing Processes, Hyderabad, India, 27-28 February 1998, pp. 127-131.
14. B. Kotiveera Chari, A. Chennakesava Reddy, Effect of Debonding on Overall Behavior of AA3003/Titanium Carbide Nanoparticulate Reinforced Metal Matrix Composites, 2nd International Conference on Composite Materials and Characterization, Nagpur, India, 9-10 April 1999, pp. 220-224.
15. H. B. Niranjan, A. Chennakesava Reddy, Effect of Particulate Debonding in AA5050/Boron Nitride Nanoparticulate Reinforced Metal Matrix Composites, 2nd International Conference on Composite Materials and Characterization, Nagpur, India, 9-10 April 1999, pp. 230-234.
16. P. M. Jebaraj, A. Chennakesava Reddy, Interface Debonding Prediction Technique for Tensile Loaded AA6061/Zirconium Oxide Nanoparticulate MMC, 2nd International Conference on Composite Materials and Characterization, Nagpur, India, 9-10 April 1999, pp. 235-239.
17. S. Sundara Rajan, A. Chennakesava Reddy, FEM Model for Volume Fraction Dependent Interface Debonding in TiN Nanoparticle Reinforced AA7020 Metal Matrix Composites, 2nd International Conference on Composite Materials and Characterization, Nagpur, India, 9-10 April 1999, pp. 240-244.
18. A. Chennakesava Reddy, Interfacial Debonding Analysis in Terms of Interfacial Tractions for Titanium Boride/AA3003 Alloy Metal Matrix Composites, 1st National Conference on Modern Materials and Manufacturing , Pune, India, 19-20 December 1997, pp. 124-127.
19. B. Kotiveera Chari, A. Chennakesava Reddy, Interfacial Debonding Analysis in Nanoparticulate Reinforced Metal Matrix Composites of AA8090/Zirconium Carbide, 2nd International Conference on Composite Materials and Characterization, Nagpur, India, 9-10 April 1999, pp. 210-214.
20. H. B. Niranjan, A. Chennakesava Reddy, Debonding Failure and Volume Fraction Effects in Nano-reinforced Composites of AA2024/Silicon Oxide, 2nd International Conference on Composite Materials and Characterization, Nagpur, India, 9-10 April 1999, pp. 215-219.
21. P. M. Jebaraj, A. Chennakesava Reddy, Analysis of Debonding along Interface of AA4015/Magnesium Oxide Nanoparticulate Reinforced Metal Matrix Composites, 2nd International Conference on Composite Materials and Characterization, Nagpur, India, 9-10 April 1999, pp. 225-229.